buildings

Article

The Influence of Vertical Arrangement and Masonry Material of Infill Walls on the Seismic Performance of RC Frames

Jingchang Kong [1], Yuhan Su [1], Zhi Zheng [2], Xiaomin Wang [3,4,*] and Yukang Zhang [1]

1 School of Civil Engineering, Yantai University, Yantai 264005, China; kjch8811@126.com (J.K.); syhtx123@foxmail.com (Y.S.); zyk5418@foxmail.com (Y.Z.)
2 College of Civil Engineering, Taiyuan University of Technology, Taiyuan 030024, China; zhengzhi@tyut.edu.cn
3 Key Laboratory of Earthquake Engineering and Engineering Vibration, Institute of Engineering Mechanics, China Earthquake Administration, Harbin 150080, China
4 Key Laboratory of Earthquake Disaster Mitigation, Ministry of Emergency Management, Harbin 150080, China
* Correspondence: xiaomin_wang@iem.ac.cn

Abstract: This study presents a finite element (FE) model, the accuracy of which is verified by the comparison between the numerical and test results. The calibrated model is used to investigate the influence of vertical arrangement and masonry material of infill walls on the seismic performance of reinforced concrete (RC) frames through pushover analysis and time–history analysis. The lateral capacity, interstorey drift ratio, and plastic hinge distribution of structures is discussed. It was found that the damage of frames with irregular vertical infill arrangement is more serious than that of bare frames, which should be limited in the seismic design process. Moreover, the disadvantages induced by the elastic modulus of masonry material should be considered in the seismic design and assessment of the frames with vertical irregularly arranged infill.

Keywords: infilled RC frame; masonry; vertical arrangement; seismic performance

check for updates

Citation: Kong, J.; Su, Y.; Zheng, Z.; Wang, X.; Zhang, Y. The Influence of Vertical Arrangement and Masonry Material of Infill Walls on the Seismic Performance of RC Frames. *Buildings* **2022**, *12*, 825. https://doi.org/10.3390/buildings12060825

Academic Editors: Jiulin Bai, Wei Guo and Junxian Zhao

Received: 14 May 2022
Accepted: 7 June 2022
Published: 14 June 2022

1. Introduction

Infill walls are widely used in RC frames as interior partitions and exterior enclosures. The poor performance of infilled RC frames has been reported in the investigation of past earthquakes such as the Wenchuan earthquake [1] and the Yushu earthquake [2]. Under actual seismic action, infill walls interact with the surrounding frames and have a significant impact on the seismic performance of RC frame structures [3]. The presence of Infill walls alter the dynamic characteristics of the structure [4], including lateral stiffness, lateral load capacity, and natural vibration period. Over the past decades, a large amount of research on the effects of configuration [5–7] and the openings [5,8,9] of infilled walls on the seismic performance of RC frames has been conducted.

In fact, infill walls are usually arranged irregularly in a vertical direction due to different architectural functions. In a building, several floors may be divided into small rooms by infill walls, while other floors may be designed as larger spaces for parking, or conference rooms. The irregular vertical arrangement of infill walls results in nonuniform distributions of lateral stiffness. Therefore, it is important to study the effect of the vertical arrangement of infill walls on the seismic performance of RC frames. Chen et al. (2019) investigated the seismic response of vertical irregular RC frames under different sites and fortification intensities [10]. Mondal and Tesfamariam (2013) studied the effects of the vertical irregularity and thickness of unreinforced infill walls on the robustness of RC-framed buildings [11]. Gong et al. (2019) compared the seismic performance of pilotis with bare RC frame structures by shaking table tests [12].

There are many kinds of blocks made of different materials. Different materials have different mechanical properties such as elastic modulus and compressive strength. It is necessary to study the effect of different masonry materials on the seismic performance of RC frames. Kakaletsis and Karayannis (2006) studied the influence of clay brick and ceramsite block infill walls on the seismic performance of RC frames [13]. Pan et al. (2018) investigated the efficiency of various retrofitting schemes using carbon-fiber-reinforced polymers in improving the seismic performance of a masonry-infilled RC frames [14]. Andreas (2009) studied the influence of unreinforced concrete infill walls on the seismic performance of RC frame structures [15].

With the development of the finite element method, some refined fine finite element models were proposed for simulating the behavior of infilled frames. Unfortunately, they were not suitable for the analysis of multistorey and multibay structures because of the large amount of calculation [16–18]. Therefore, some simplified analysis models [9,19,20] were proposed. Polyakov (1956) proposed an equivalent diagonal bracing model in the analysis of the failure mechanism of the infill walls [21]. The effective width of the equivalent brace is the key parameter, and it is difficult to determine. Holmes (1961) recommended that the effective width of the equivalent brace be one third of the diagonal of the infill wall [3]. However, the single strut is insufficient to describe the interaction between RC frames and infill walls. Many researchers have proposed multiple strut models to simulate the wall–frame interaction effect [22–24]. Fiore et al. (2012) simulated the complex behavior of infilled frames under lateral loads using two equivalent struts [24]. EI-Dakhakhni (2003) presented an equivalent three struts based on the failure modes of masonry-infilled frames [25]. Furtado et al. (2017) simulated the seismic behavior of infill walls with or without openings by using a five-strut model [26].

In order to investigate the influence of the vertical arrangement and masonry material of infill walls on the seismic performance of RC frames, six RC frames with different arrangements of infill walls were designed. A five-strut simplified model was utilized to simulate the seismic contribution of the infill wall, and three-dimensional finite element models were built in OpenSees (v3.2.1, UC, Berkeley, Berkely, CA, USA). Then, the pushover analysis and time–history analysis were performed, and the base shear-top displacement relation, development of plastic hinges, and interstorey drift ratio are discussed to evaluate the seismic performance of the structure.

2. Design Information of Infilled RC Frames

A six-storey and three-bay RC frame structure was designed according to the Chinese seismic design codes [27,28]. Dead load is 5 kN/m^2 and live load is 2 kN/m^2. The fortification intensity is VII (the design acceleration is 0.1 g) and the site classification is II. The plan and elevation are shown in Figure 1. The arrangement of beams in each storey is illustrated in Figure 2, in which Bxn and Byn represent the beams in the two directions. The section of beams in x and y directions are 200 $\times$ 400 mm^2 and 250 $\times$ 500 mm^2, respectively. The concretes C30 and C35 are used for columns and beams, respectively. The reinforcements HRB 400 and HPB 300 are used for the longitudinal bar and stirrup, respectively. The design information of columns and beams is listed in Tables 1 and 2, respectively. The stirrups in all the beams are A8@100/150. The mechanical properties of the concrete and steel bar are described in Table 3.

Table 1. Sizes and reinforcement details of frame columns.

Storey	Section Size (mm^2)	Steel Bars Area (mm^2)	Stirrup
1–2	600 $\times$ 600	2240	,8@100/150
3–4	550 $\times$ 550	2538	,8@100/150
5–6	500 $\times$ 500	2324	,8@100/150

Table 2. Sizes and reinforcement details of frame beams.

Storey	Steel Bars Area (mm^2)					
	Bx1 Bx4 Bx9 Bx12	Bx2 Bx3 Bx10 Bx11	Bx5 Bx8	Bx6 Bx7	By1 By5 By9 By4 By8 By12	By2 By6 By10 By3 By7 By11
1	1112	1226	710	1080	1018	1269
2	1269	1222	1018	1080	1018	1256
3	1018	1166	804	1030	770	2393
4	817	1018	710	971	910	1030
5	911	1018	804	804	910	1273
6	804	804	804	804	804	804

Table 3. The mechanical properties of reinforcements and concrete.

Material	Elastic Modulus (GPa)	Yield Strength (MPa)	Compressive Strength (MPa)
HPB300	210	300	270
HRB400	200	400	360
C30	30	-	14.3
C35	31.5	-	16.7

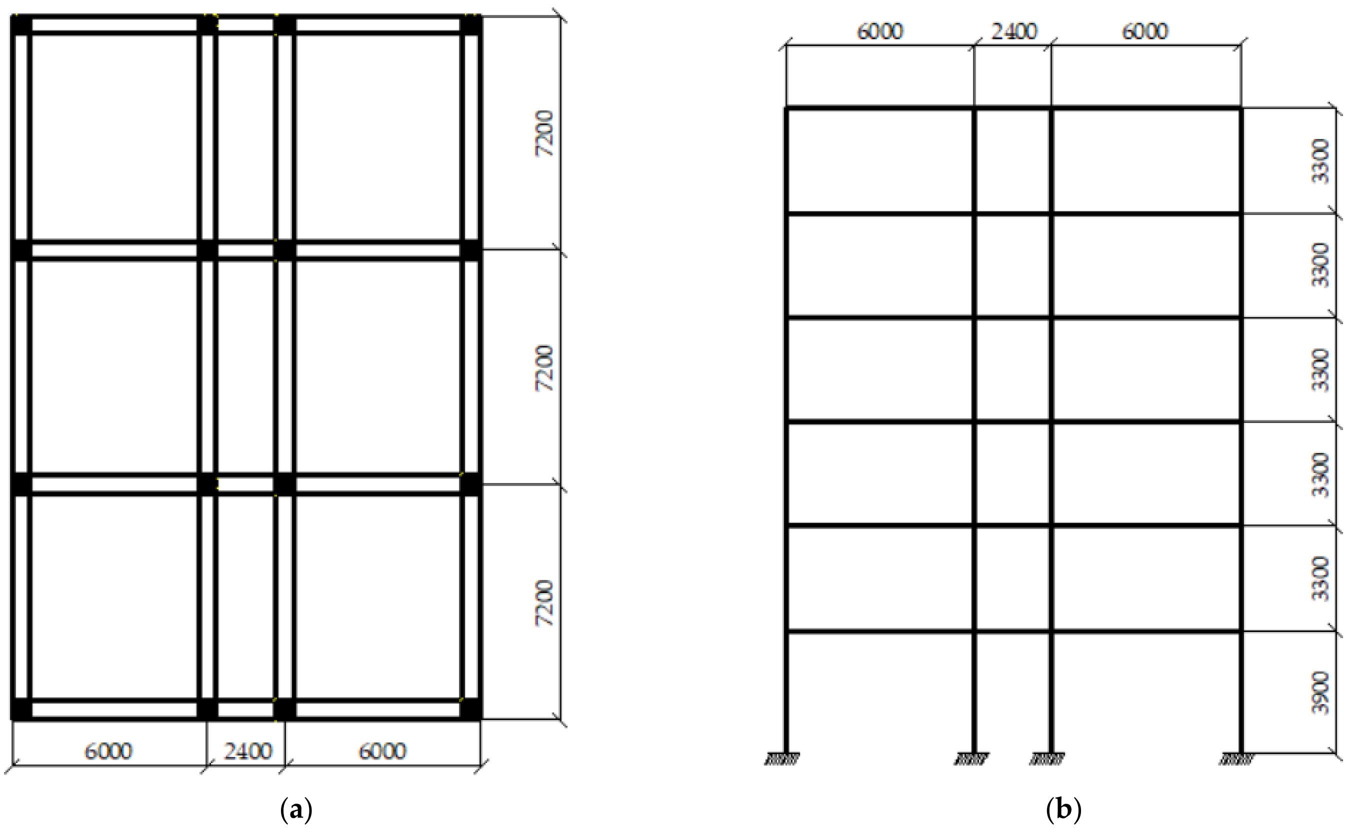

Figure 1. The plan and elevation of the RC frame (unit: mm): (**a**) plan view; (**b**) elevation.

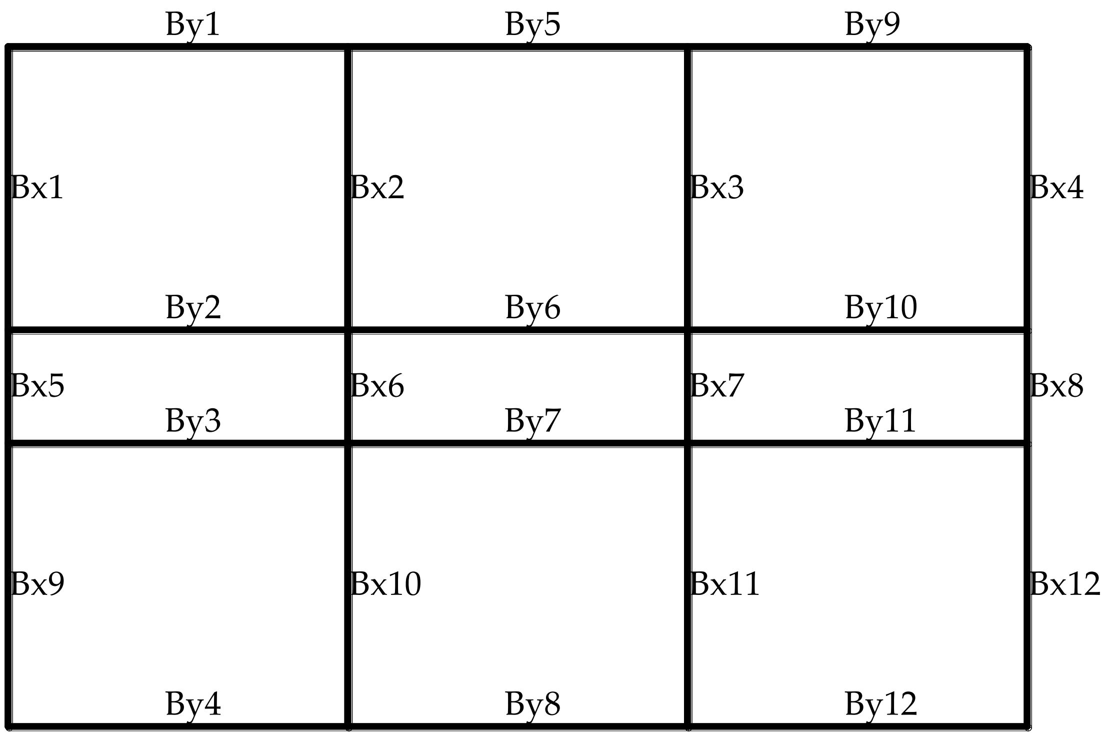

Figure 2. The arrangement of beams.

Since infill walls are always arranged irregularly along the height of the building to accomplish different functions, six models with different infill wall arrangements were analyzed, as described in Figure 3. Model M1 is the bare frame. Model M2 is the frame with infill walls on all the storeys. Model M3 is the frame without infill walls on the first two storeys. Model M4 is the frame without infill walls on the third and fourth storeys. Model M5 is the frame without infill walls on the top two storeys. Model M6 is the frame without infill walls in the middle bay.

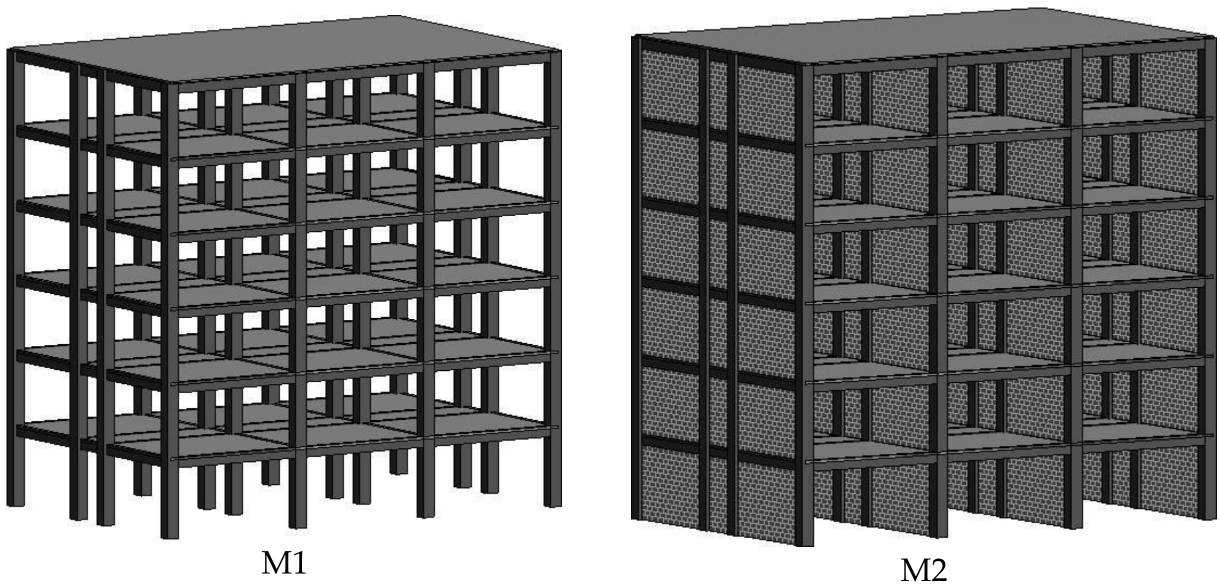

Figure 3. *Cont.*

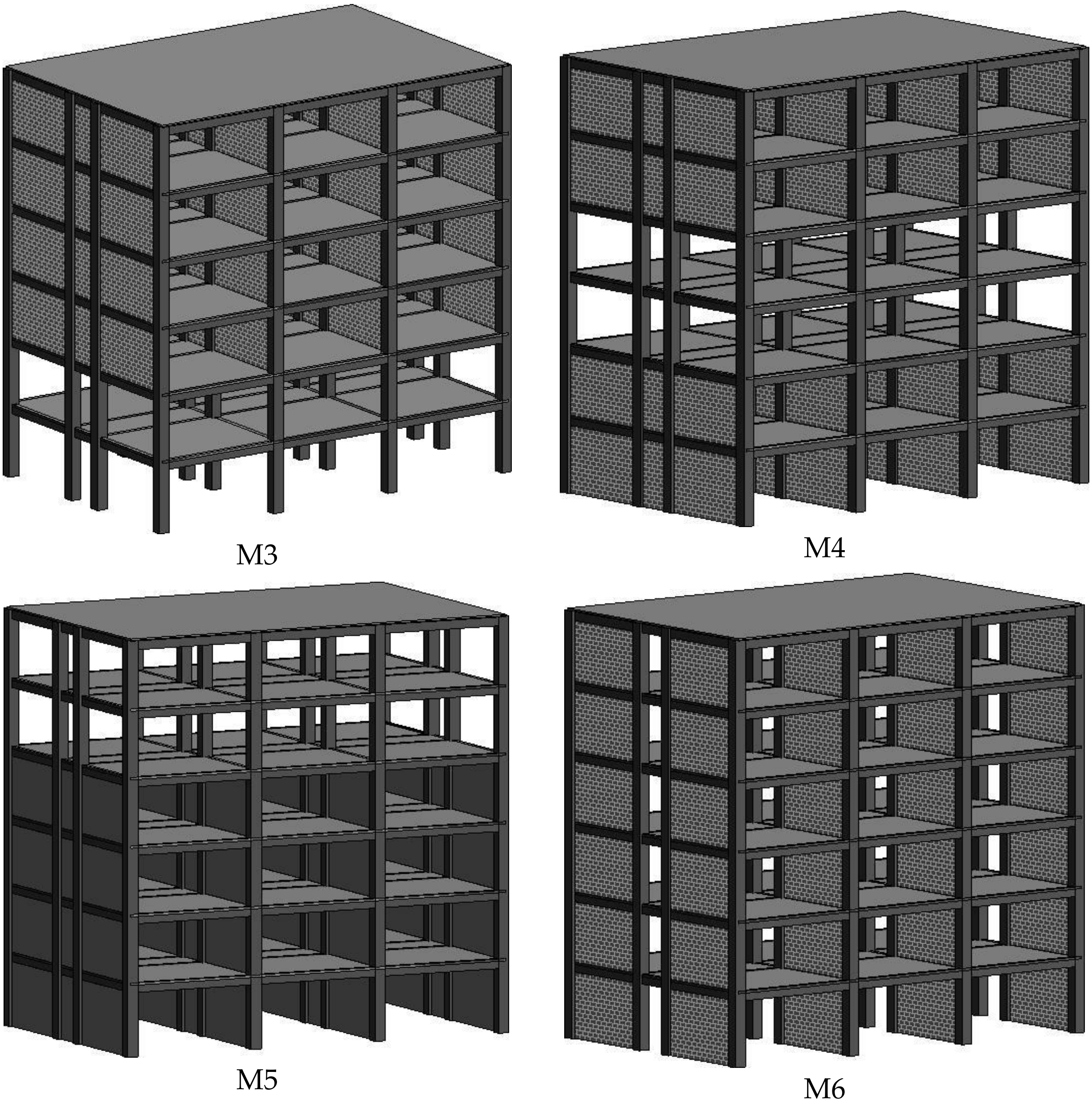

Figure 3. The six models with different infill wall arrangements.

In addition, four different masonry blocks were adopted as infill wall material to investigate the effect of material property on the seismic performance of the frame structure. The masonry blocks, named as I1, I2, I3, and I4, are fired common brick, hollow clay brick, concrete hollow block, and ceramsite concrete block, respectively. The mechanical properties of the four masonry materials are listed in Table 4.

Table 4. The mechanical property parameters of masonry material.

Material Number	Elastic Modulus (MPa)	Compressive Strength (MPa)	Shear Strength (MPa)	Bulk Density (kg/m^3)
I1	5672	6.1	0.7	1800
I2	4441	4.15	0.63	1800
I3	3720	3.48	0.69	2000
I4	2751	3.42	0.32	1800

3. Finite Element Modeling Technique

3.1. Modeling of Frames and Infill Walls

In this paper, the finite element modeling of six-storey RC frames was carried out in OpenSees. A displacement-based beam–column element was adopted to simulate the behavior of the frame beams and columns. The fiber section was used for element section. Material Concrete 02 was used to simulate the behavior of the concrete, and material Steel 02 was adopted for the reinforcement.

The five-strut model proposed by Furtado and Rodrigues (2016) was used for simulating the behavior of infill walls [29]. The model considers the interaction between the infill and the surrounding RC frame, which can accurately reflect the structural response influenced by the infill wall. The five-strut model, as shown in Figure 4, consists of four diagonal struts with rigid behavior and a central strut element with the nonlinearity hysteresis behavior concentrated. The model can combine material, section, and element. The effective width, a, of the elastic plastic central strut of the five-strut model is calculated by the following formula:

$$a = 0.175(\lambda_1 h_{col})^{-0.4} r_{inf} \tag{1}$$

$$\lambda_1 = (\frac{E_{me} t_{inf} sin2\theta}{4E_{fe} I_{col} h_{inf}}) \tag{2}$$

where h_{col} is the height of column, h_{inf} and t_{inf} are the height and thickness of infill walls, respectively, and E_{fe} and E_{me} are elastic modulus of the frame and infill wall, respectively. I_{col} is the moment of inertia of the column section, L_{inf} is the length of infill wall, and r_{inf} is the diagonal length of infill wall. λ_1 is the effective width parameter of infill wall. The angle $\theta = tan^{-1}\left(h_{inf}/L_{inf}\right)$.

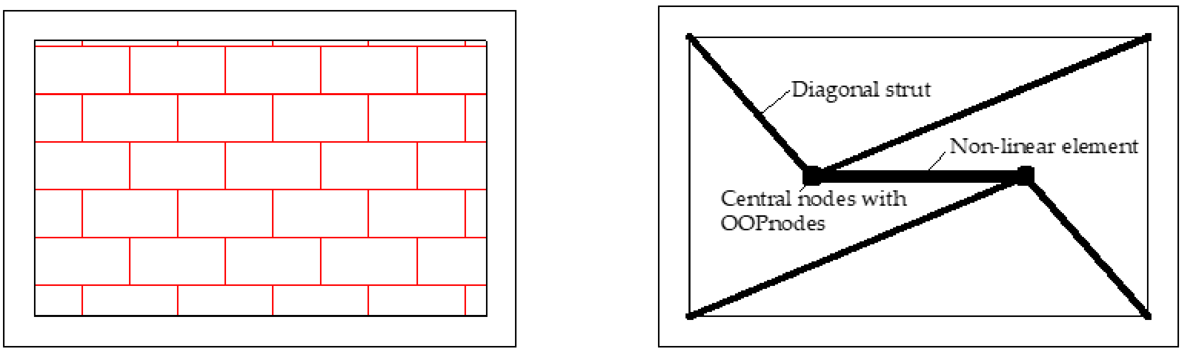

Figure 4. Five-strut model of masonry infill wall.

The nonlinear behavior of the central element is represented by the Pinching 04 model, as shown in Figure 5 [29]. The skeleton curve is defined by eight parameters (F_{max}, F_y, F_c, F_u, d_c, d_y, $d_{F_{max}}$ and d_u). The ratio between cracking and maximum force (F_c/F_{max}) is adopted as 0.55, and the cracking displacement d_c is the interstorey displacement drift ratio of 0.12%. The yielding force F_y and yielding displacement d_y are determined as the intermediate point between the cracking point (F_c, d_c) and the maximum point (F_{max}, d_{max}). The maximum force (F_{max}) occurs approximately between the interstorey displacement drift ratio of 0.25% and 0.5%, and $d_{F_{max}}$ is taken as 0.5% in this study. The residual force F_u is about 20% of the maximum force. The residual displacement (d_u) is five times the displacement at the maximum force. The maximum force F_{max} can be calculated by the following equations:

$$F_{max} = 0.818 L_{inf} t_{inf} f_{tp} c \tag{3}$$

$$c = (1 + \sqrt{c_1^2 + 1})/c_1 \tag{4}$$

$$c_1 = 1.925 \frac{L_{inf}}{h_{inf}} \tag{5}$$

where f_{tp} is the cracking strength of the masonry wall, t_{inf}, $L_{inf,}$ and h_{inf} are the thickness, length, and height of the infill wall, respectively.

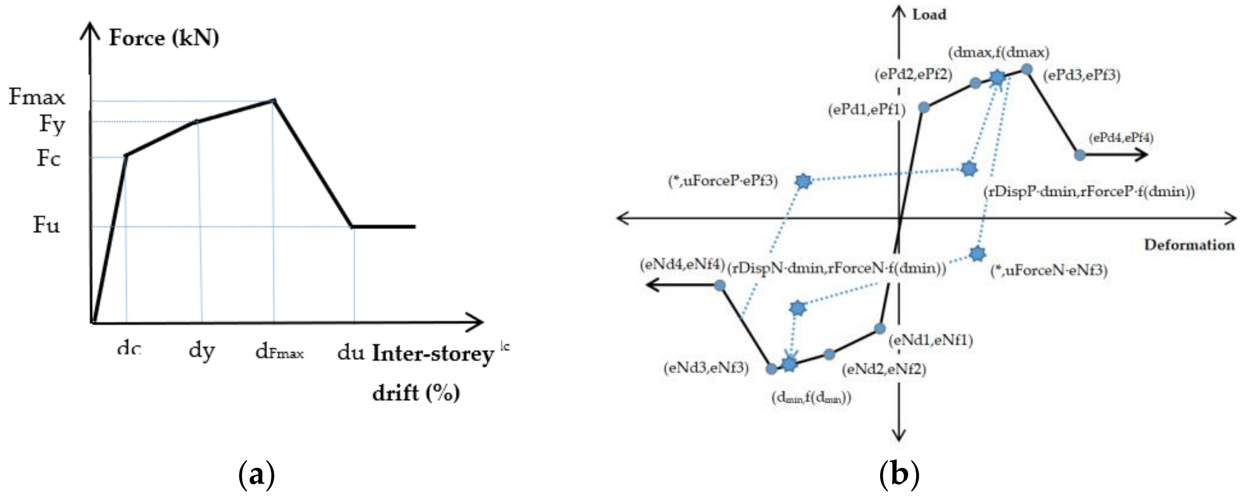

Figure 5. The nonlinear behavior of the central element: (**a**) the force–displacement relationship; (**b**) the Pinching 04 model.

3.2. *Verification of the Finite Element Modeling*

De Risi et al. (2019) [30] and Ricci et al. (2018) [31] investigated the seismic performance of unreinforced masonry-infilled RC frames by several pseudostatic tests. In this study, the specimens IP_M-OOP and IP_H-OOP in De Risi et al. (2019) [30] and the specimens IP+OOP-H in Ricci et al. (2018) [31] were adopted to verify the accuracy of the finite element model. The information of test specimens is illustrated in Figure 6. Hollow clay brick with 60% of the void ratio was chosen for construction of the infill wall. Table 5 describes the mechanical property of concrete, steel, and masonry of the three specimens. The imposed displacement history of the specimens is shown in Table 6. For each level of displacement loading, three cycles were applied on the specimen. The modeling parameters of the elastic–plastic central element for the infill wall are listed in Table 7.

Table 5. Mechanical properties of the material of test specimens.

Material Properties	Specimens IP_M-OOP and IP_H-OOP	Specimen IP + OOP-H
Concrete compressive strength (MPa)	42.90	36.00
Steel bars yielding strength (MPa)	524.50	552.00
Masonry compressive strength (MPa)	2.00	2.45

Table 6. Imposed displacement history.

Cycle Level	Interstorey Drift Ratio (%)	Displacement (mm)	Cycle Numbers
1	0.1	1.97	3
2	0.2	3.93	3
3	0.3	5.90	3
4	0.4	7.86	3
5	0.5	9.83	3
6	0.6	11.79	3

Table 7. Modeling parameters of the elastic–plastic central strut.

Strut Parameter		Specimen IP_M-OOP and IP_H-OOP	Specimen IP + OOP-H
The width of strut (mm)		647	744
Pinching 04	σ1 (MPa)	0.061	0.367
	σ2 (MPa)	0.087	0.518
	σ3 (MPa)	0.112	0.667
	σ4 (MPa)	0.022	0.133
	ε1	0.001	0.001
	ε2	0.003	0.003
	ε3	0.005	0.005
	ε4	0.025	0.025

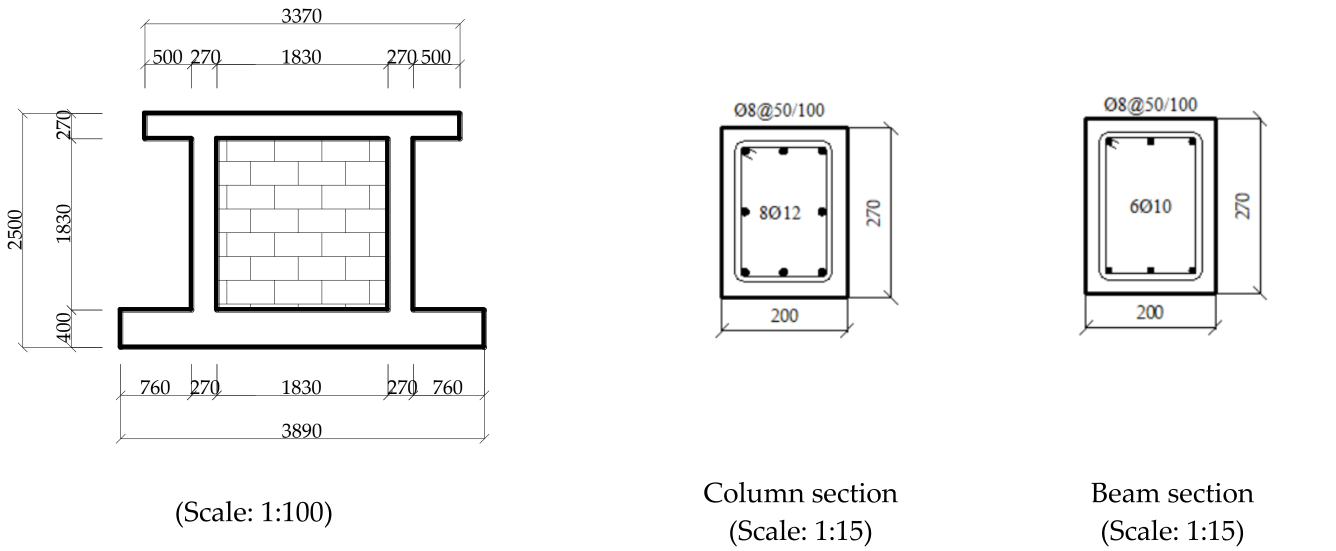

(**a**)

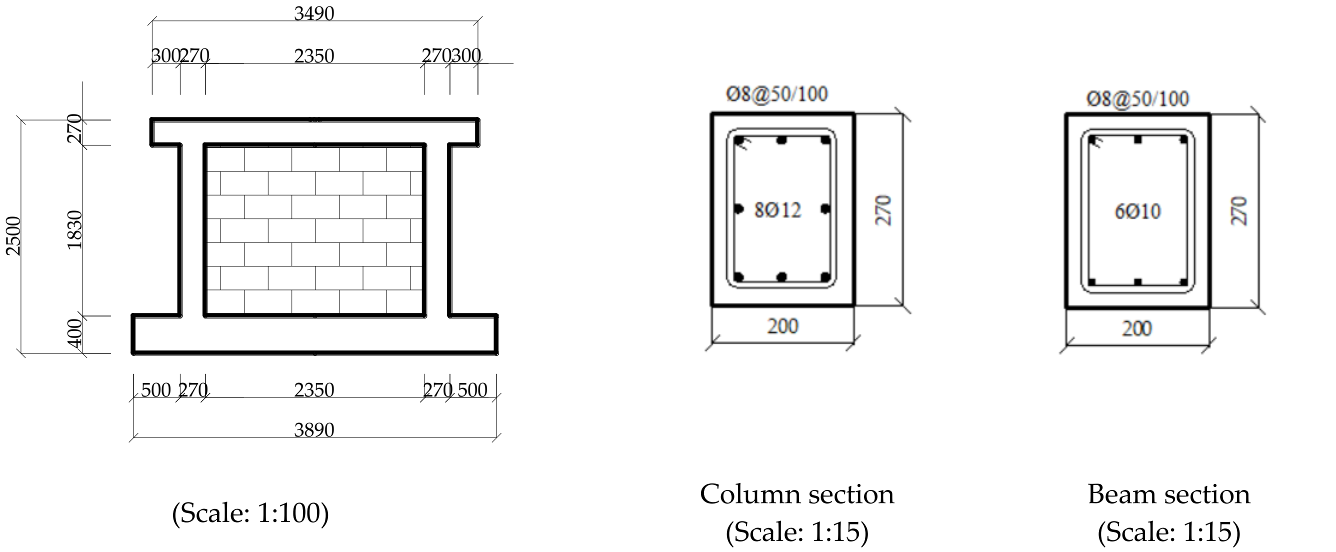

(**b**)

Figure 6. Frame size and reinforcement information: (**a**) De Risi et al. (2019) [30]; (**b**) Ricci et al. (2018) [31].

Finite element modelings of the three test specimens were built in OpenSees. The lateral load is applied to the end of beam and the loading procedure described in the test was adopted for the analysis.

The load-displacement curves of test result and numerical result for three specimens is shown in Figure 7. The comparison of the peak load and secant stiffness is listed in Table 8, in which secant stiffness is the ratio of the peak load to the corresponding displacement. It can be seen that the numerical result agrees well with the test result in terms of the general trend, load-bearing capacity, and initial stiffness. Moreover, the pinch effect of the infill wall frame specimen during the cyclic loading is also well-captured. To be specific, the average error value of bearing capacity is 2.92%, and the average error value of secant stiffness is 5.52%. One thing that should be mentioned is that the positive and negative parts of the load-bearing capacity curves of some tests are quite asymmetrical, and it is not reflected in the numerical results. In general, it is believed that the model used in this study can simulate the seismic performance of infilled frame structures accurately.

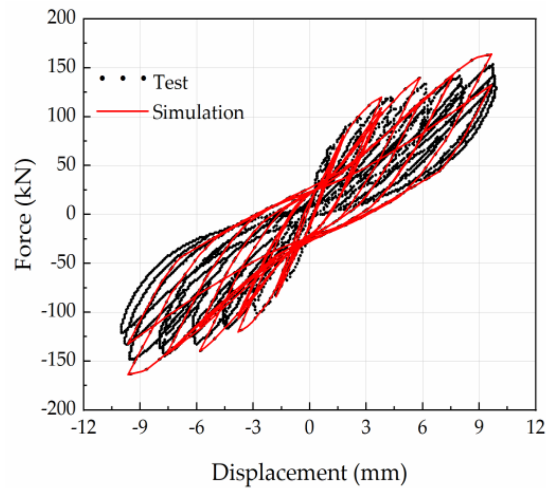

(a)

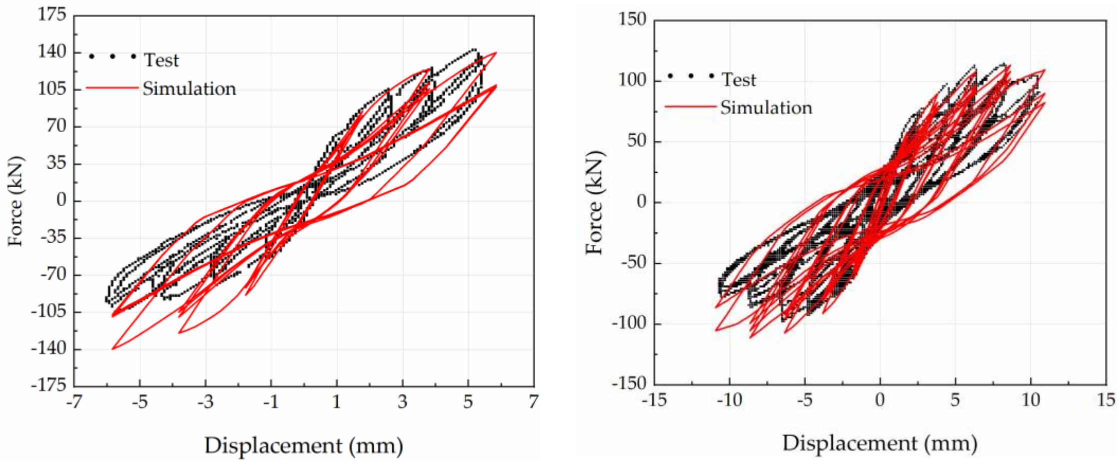

(b) (c)

Figure 7. The load-displacement responses of numerical and test results. (**a**) The result of IPM-OOP. (**b**) The result of IPH-OOP. (**c**) The result of IP + OOP-H.

Table 8. Comparison between numerical and test stiffness and load-carrying capacity.

Specimen		IPM-OOP	IPH-OOP	IP + OOP-H
Peak load (kN)	Test	142.60	152.60	112.30
	Simulation	140.45	162.76	112.95
	Error	1.51%	6.66%	0.58%
Secant stiffness (kN/mm)	Test	5.10	9.70	8.40
	Simulation	5.80	9.70	8.64
	Error	13.70%	0.00%	2.86%

4. Pushover Analysis

Pushover analysis is widely used for structural seismic analysis. In this study, the pushover analysis of six RC frame models with different infill arrangements was first carried out. An inverted triangular distributed loading scheme was adopted, which is determined according to the following formula:

$$F_i = \frac{G_i H_i}{\sum_{j=1}^{N} G_i H_i} V_b \quad (6)$$

where F_i is the lateral load applied to the ith storey, G_i is the gravity load of ith storey, Hi is the height of the ith storey, and V_b is the base shear of the structure.

4.1. Pushover Capability Curve

The base shear-top displacement curves of six frame models are obtained and shown in Figure 8. Among all the models, the bare frame (M1) has the lowest load-bearing performance, including the peak load value and initial stiffness, while the fully infilled frame (M2) has the highest load bearing performance, whose peak load value is approximately 6.2 times that of the M1. The performance curves of the other models are in between the curves of these two models. For the frame with an absence of infill walls at the first two storeys (M3), the lateral load capacity is 80% lower than that of M2, which is only slightly higher than that of M1. As the storeys with an absence of infill walls move up, the lateral capacity of the model gradually increases by comparing the responses of M3, M4, and M5. The lateral capacity of M5 is about 160% larger than that of M3. For M6, with an absence of infill walls in the middle bay, its lateral capacity is about 65% of that of M2 but is larger than that of M3, M4, and M5. Therefore, it seems more dangerous to have the absence of infill walls in a vertical direction than to have the absence of infill walls in a horizontal direction.

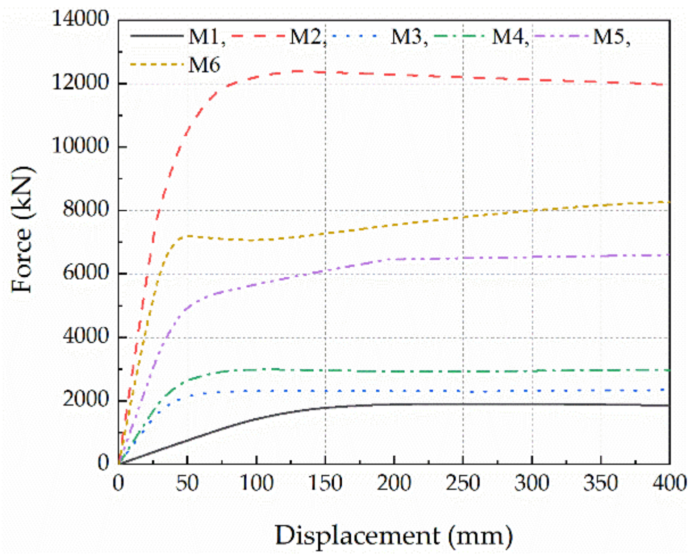

Figure 8. The base shear-displacement curves of six models.

4.2. Interstorey Draft Ratio

The performance points of pushover capability curves were obtained by the capacity spectrum method. The corresponding interstorey drift ratio for the models are shown in Table 9 and Figure 9. Compared with the result of M1, the interstorey drift ratio of M2 is decreased by more than 57%. The performance of the bare frame is improved because of the full arrangement of infill walls in M2. For the models with irregular vertical arrangement, M3, M4, and M5, the storeys with an absence of infill walls form the weak storeys due to the sharp drop in lateral stiffness. Therefore, the maximum interstorey drift ratios occur at the storeys without infill walls. As the storeys without infill walls move up, the maximum interstorey drift ratio is correspondingly decreased. That means the maximum interstorey drift ratio of M5 is smaller than that of M3 and M4. In fact, the maximum interstorey drift ratio of M5 is even 16% larger than that of M1, which is quite undesirable. The interstorey drift ratio of M6 is relatively small, which is very close to that of the fully infilled frame M2, since the lateral stiffness of M6 is distributed uniformly.

Table 9. The interstorey drift ratio of models at the performance point.

Storey	M1	M2	M3	M4	M5	M6
6	1/855	1/1031	1/3002	1/2609	1/370	1/1013
5	1/360	1/769	1/2633	1/2254	1/196	1/662
4	1/267	1/617	1/2546	1/175	1/1369	1/546
3	1/221	1/541	1/2621	1/155	1/1435	1/472
2	1/227	1/535	1/144	1/2827	1/1622	1/437
1	1/361	1/870	1/150	1/4285	1/2573	1/459

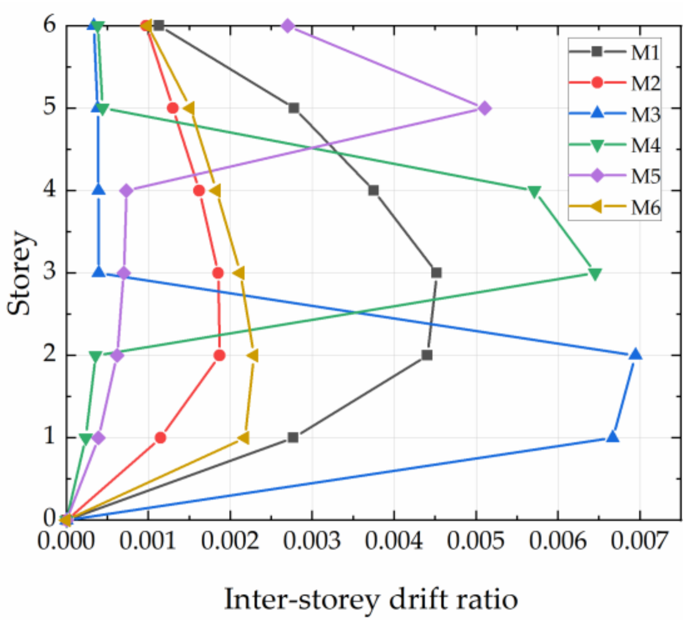

Figure 9. The interstorey drift ratio of six models at the performance point.

4.3. Distribution of the Plastic Hinge

The distribution of the plastic hinge of six frame models with different arrangements of infill walls at the maximum interstorey drift ratio of 2% (collapse limit state) is shown in Figure 10. The serial numbers in each figure represents the order of plastic hinge occurrence. As shown in Figure 10a, the plastic hinges are developed at the ends of most beams of the bare frame M1 and at the bottom of the bottom columns. The number of plastic hinges developed in the M2 is 24% fewer than that of M1 because the regular arrangement of infill walls in frames increases the lateral stiffness and decreases the deformation of the frame structure. For the models M3, M4, and M5 with an irregular arrangement of infill walls in the vertical direction, plastic hinges usually occur firstly at the ends of beams at the storeys with the absence of infill walls. As the lateral load continued to increase, the plastic hinges gradually occured at the ends of columns on the same storeys. Due to the irregular arrangement of infill walls, the lateral stiffness of the storeys without infill walls is much smaller than that of the adjacent upper and lower storeys, which forms weak storeys. The deformation is concentrated in these weak storeys, and the damage is also concentrated in these storeys. For the frame without infill walls in the M6 midspan, the plastic hinges first occur at the beam ends of the midspan. After most of the midspan beams have plastic hinges, plastic hinges begin to occur at the column and beam ends at the bottom of the structure.

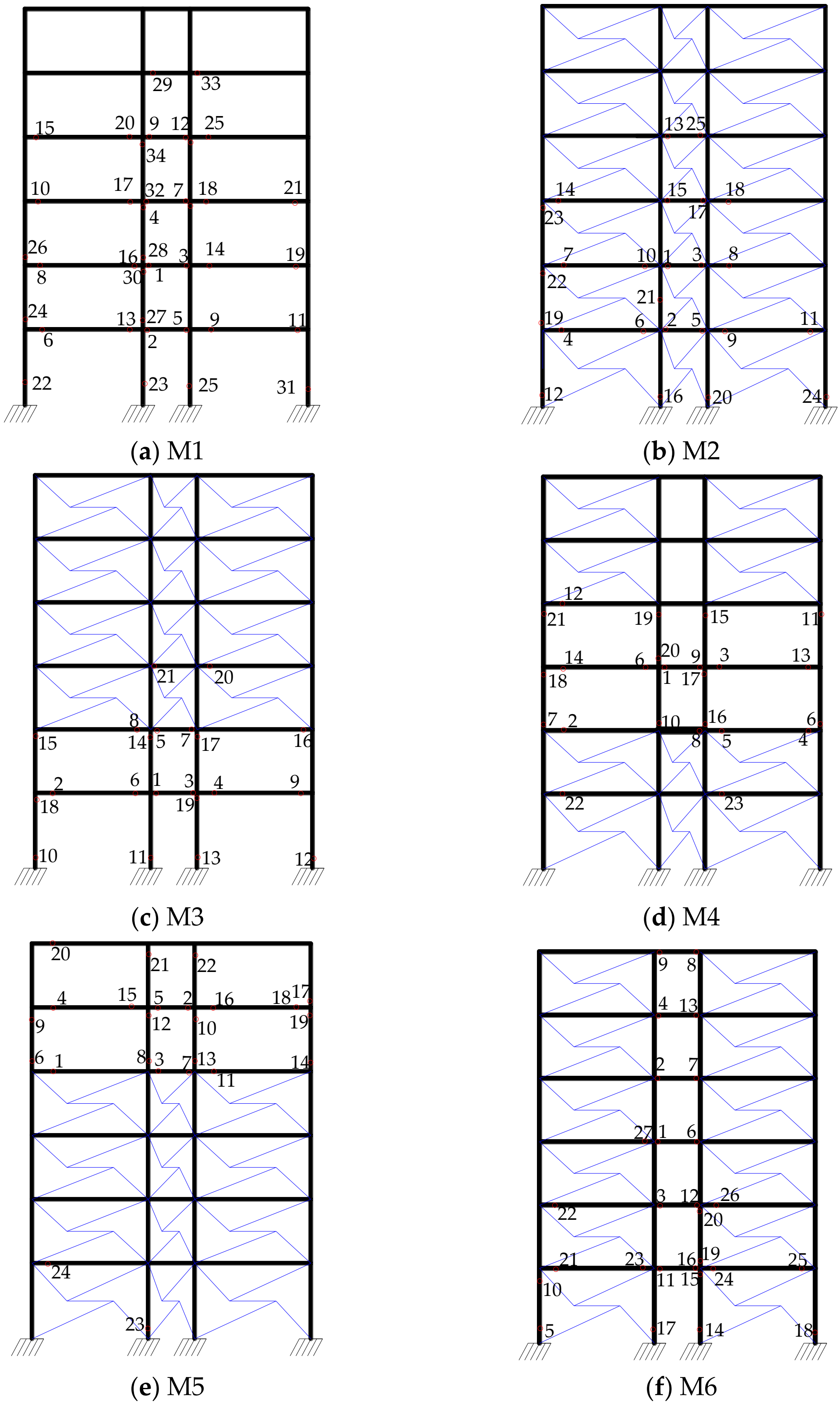

(**a**) M1 (**b**) M2 (**c**) M3 (**d**) M4 (**e**) M5 (**f**) M6

Figure 10. Plastic hinge distribution of six models. (Note: red circles represent plastic hinges).

5. Nonlinear Dynamic History Analysis

5.1. Selection of the Ground Motion

According to the Chinese seismic code [27], a suit of appropriate ground motions consisting of actual recorded accelerograms and artificially simulated accelerograms shall be selected based on site class and the design earthquake group. Thereinto, the quantities of the actual recorded accelerograms shall not be less than 2/3 the total of ground motions. Effective duration shall be 5–10 times that of the basic period of the structure. In this paper, two sets of representative and typical strong ground motion records, and an artificial ground motion record which is obtained using simulation method, were selected. The records and the corresponding parameters can be seen in Table 10 and Figure 11. According to the Chinese code [27], the peak ground acceleration is 220 cm/m^2 for a field of an VII seismic intensity rare earthquake. Therefore, the three ground motion records are scaled to 220 cm/m^2 as the peak acceleration.

Table 10. The parameters of ground motion records.

Ground Motion Records	Time Lag (s)	Total Time (s)	Peak Acceleration (cm/s^2)
Artificial	0.01	30	431.20
Taft	0.02	54.38	152.58
Tang Shan	0.01	59.92	55.49

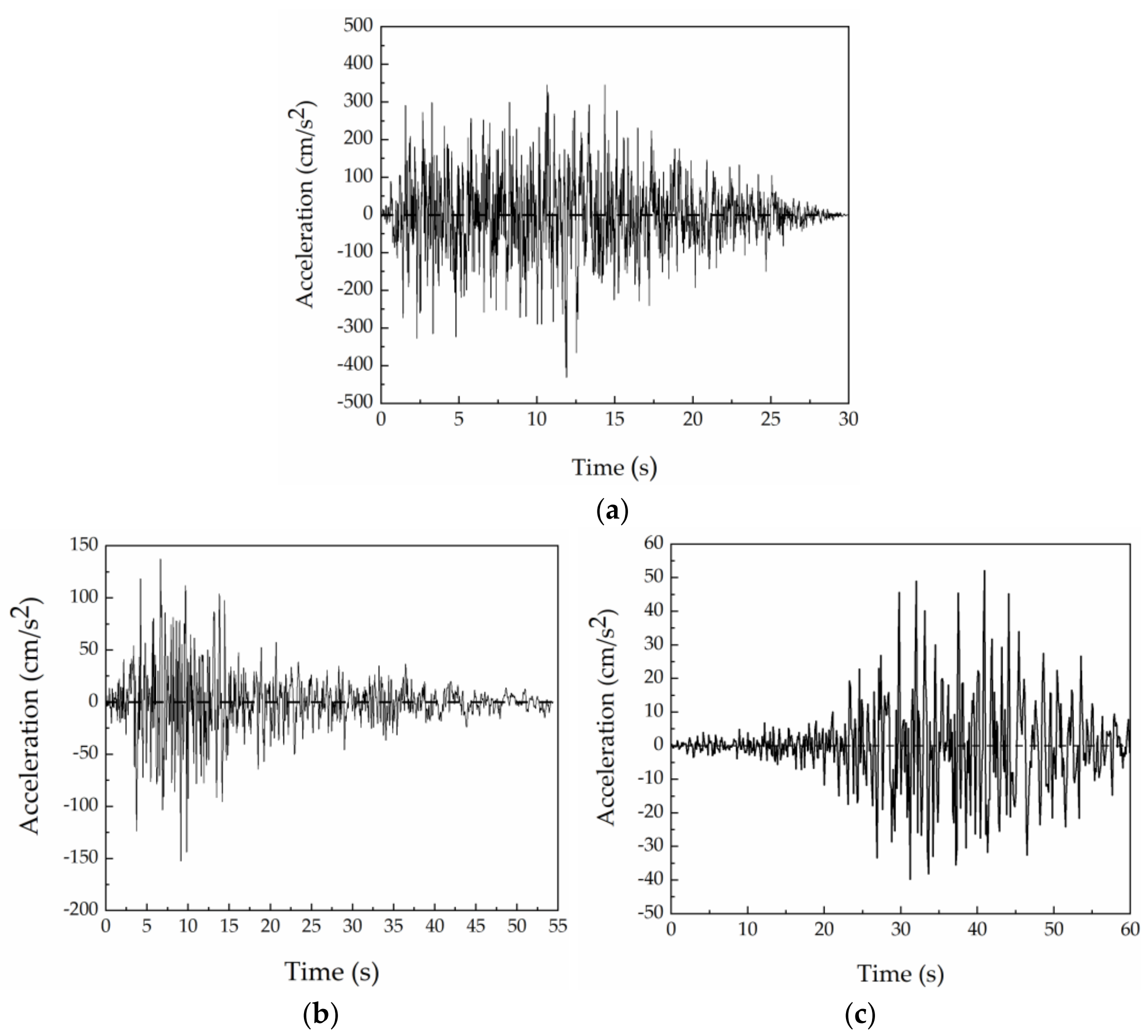

Figure 11. The earthquake ground motions: (**a**) Artificial ground motion record; (**b**) Taft ground motion record; (**c**) Tang Shan ground motion record.

5.2. The Influence of Different Vertical Irregularities

5.2.1. Base Shear

The maximum base shear of the six models under the three earthquake ground motions are shown in Table 11. By comparison, the peak base shear of M2 was at least three times bigger than that of M1, and the peak of the base shear of M6 is a little lower (15–25%) than that of M2. The absence of infill walls at the base storey decreases the base shear 56–70% compared with M2. Compared with structures M3, M4, and M5, the maximum base shear of the structure increases with the upward storeys with an absence of infill walls. With the absence of infill walls, the lateral stiffness of the storey decreases, and the seismic capacity of the structure also decreases. The vertical irregularities of infill walls lead to the discontinuity of stiffness. When the structure is subjected to external force, there is a large deformation at the discontinuity of stiffness. That may lead to structural collapse before the other components yield. Although there are not infill walls in the middle bay of M6, the peak base shear is quite close to the vertical regularity of infill walls.

Table 11. The peak base shear of six models under the ground motions. (unit: kN).

Ground Motion	M1	M2	M3	M4	M5	M6
Artificial	843.11	4426.41	1945.96	2105.47	2798.06	3361.05
Taft	1399.55	6516.39	1926.01	2409.87	3975.50	5232.79
Tangshan	1574.44	5867.07	1998.29	2091.17	2785.77	5043.30

5.2.2. Interstorey Drift Ratio

As shown in Figure 12, the interstorey drift ratio of models with six different infill arrangements under the three different ground motions are given. The discontinuity of the interstorey drift ratio is consistent with the position of storeys with an absence of infill walls. Although there are not infill walls in the middle bay of M6, its vertical arrangement is relatively regular. Therefore, there is not an abrupt change in the vertical development of interstorey drift ratio. By comparison, between M1 and others, the existence of infill walls takes an essentially difference influence on structural seismic performance. The interstorey drift ratio of M3 is the biggest (about 0.95%) under all three ground motions. This result means that the base storey of the structure with an absence of infill walls is detrimental to its seismic performance.

5.3. The Influence of Masonry Material

The seismic performance of infill walls made of four kinds of material was investigated using the finite element software OpenSees. The mechanical properties of material can be seen in Table 4. The effective width of equivalent struts of simplified models for different material, calculated according to Equation (1), are presented in Table 12.

Table 12. The effective width of equivalent struts of simplified models.

Material	6 m Bay Infill Wall (m)	2.4 m Bay Infill Wall (m)
fired common brick (I1)	0.672	0.409
hollow clay brick (I2)	0.714	0.434
concrete hollow block (I3)	0.724	0.440
haydite concrete block (I4)	0.740	0.450

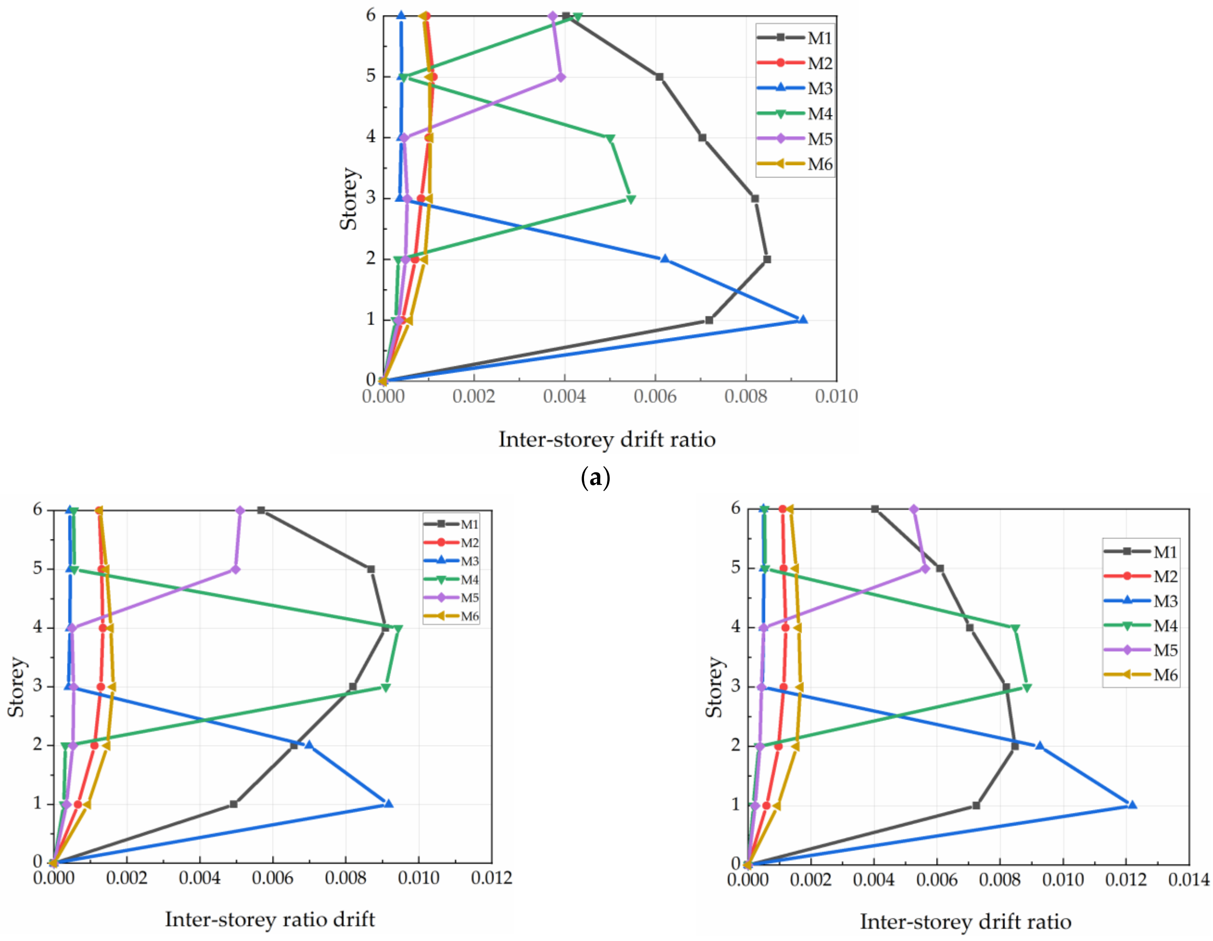

(**a**)

(**b**) (**c**)

Figure 12. Interstorey drift ratio of six models under three ground motions: (**a**) for artificial ground motion; (**b**) for taft ground motion; (**c**) for Tang Shan ground motion.

The seismic performance of frames infilled with walls of different materials is investigated. The maximum base shear of each structure under three ground motions is shown in Table 13. It can be seen that the base shears of models with infill walls consisting of any kind of material are larger than that of the bare frame. The result means that the infill walls can contribute important lateral bearing capacity despite the relative weak masonry material. The base shear of structures with infill walls made of fired common bricks (I1) is larger than that of concrete hollow bricks (I3) because the elastic modulus and compressive strength of I1 is higher than that of I3. However, improving the mechanical property of infill wall material is not enough to improve the seismic performance of infilled RC frames because of the discontinuity of stiffness caused by the absence of infill walls. The base shear of M2I3 is larger than that of other structures infilled with material I1, expect the structure M2I1, and a similar result can be seen from Table 13.

Table 13. The maximum base shear under three ground motions.

The Maximum Base Shear under Artificial Ground Motion (kN)				
	I1	I2	I3	I4
M2	4426.41	3379.84	3510.28	3649.39
M3	1945.96	1707.61	1790.43	1828.73
M4	2105.47	1654.35	1866.29	1925.74
M5	2798.06	2602.50	2712.48	2743.33
M6	3361.05	2813.73	2825.93	2884.75

Table 13. *Cont.*

The Maximum Base Shear under Taft Ground Motion (kN)				
M2	6516.39	5725.19	5732.36	6042.32
M3	1926.01	1939.32	1925.34	1929.98
M4	2409.87	2152.83	2307.79	2352.28
M5	3975.50	3620.29	3520.40	3711.37
M6	5232.79	4307.29	3953.42	4175.20
The Maximum Base Shear under Tang Shan Ground Motion (kN)				
M2	5867.07	4926.00	5177.28	5367.67
M3	1998.29	1965.53	1978.55	1984.04
M4	2097.17	2108.31	2080.68	2078.49
M5	2785.77	2785.52	2977.52	2972.62
M6	5043.30	4321.50	4078.69	4268.52

The interstorey drift ratio of models under taft ground motion is shown in Figure 13. As can be seen from Figure 13a,e, with elastic modulus of material decreased (from I1 to I4), the interstorey drift ratio of models (M2 and M6) with vertical regularity is increased gradually. The elastic modulus of material I is about 50% lower than that of the material I1, but the interstorey drift ratio is 22% and 19% larger, for M2 and M6, respectively. Nevertheless, the interstorey drift ratio of models (M3, M4, and M5) with vertically irregular infill arrangement is decreased gradually because of the smaller infill elastic modulus, as shown in Figure 13b,d. For M4, the interstorey ratio is 11% smaller due to the fact that the elastic modulus of material decreases 50%. Therefore, it is very important to choose reasonable infill wall masonry material and reasonable infill wall arrangement in the seismic design of structures.

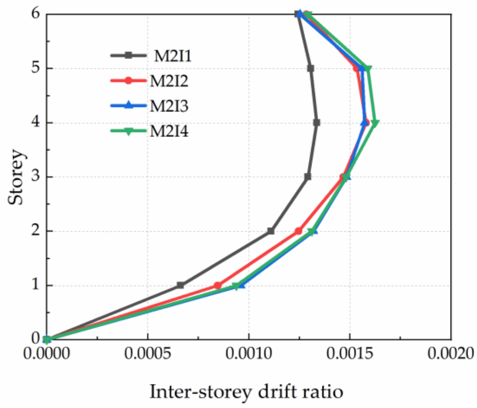

(**a**)

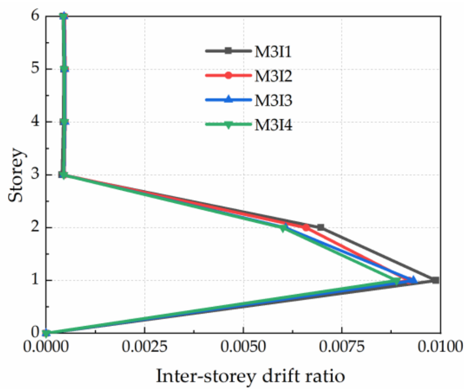

(**b**)

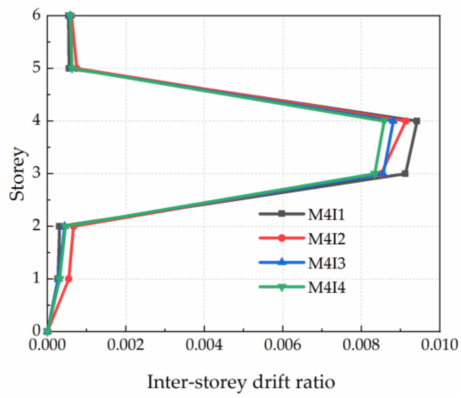

(**c**)

Figure 13. *Cont.*

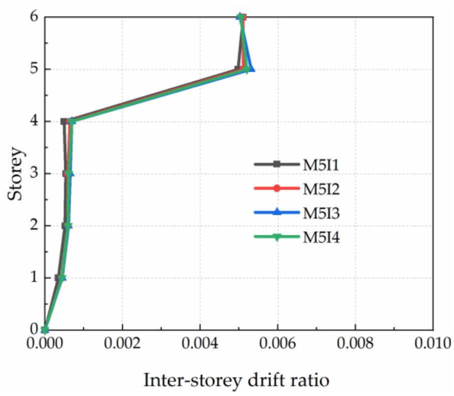

(**d**)

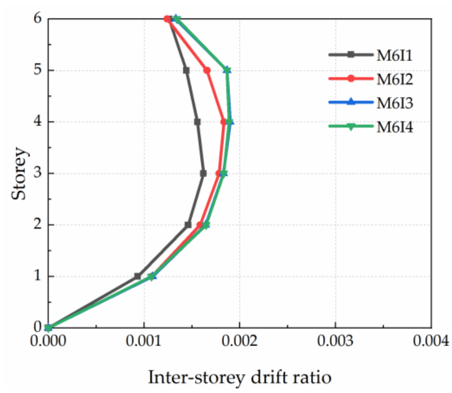

(**e**)

Figure 13. The interstorey drift ratio of different models under taft ground motion: (**a**) M2; (**b**) M3; (**c**) M4; (**d**) M5; (**e**) M6.

6. Conclusions

This manuscript investigates the seismic performance of multistorey RC frames, with special focus on the effect of vertical arrangement and masonry material of infill walls. A five-strut simplified model of infill wall is validated by the experiments. Then, through the static elastic–plastic analysis, the base shear, the interstorey drift ratio, and the plastic hinge distribution of frames with different vertical infill wall arrangements were studied. Finally, according to the nonlinear dynamic history analysis under three different earthquake ground motions, the base shear and interstorey drift ratio of structures were investigated. The following conclusions are drawn from this study:

(1) Pushover analysis is carried out on infilled RC frames, considering different vertical arrangements. Compared with the bare frame (M1), the regular vertical infill-arranged wall in the RC frames (M2 and M6) can improve the overall bearing capacity and stiffness of the structure greatly and decrease the interstorey drift ratio more than 57%. Additionally, the number of plastic hinges of M2 decreases 24% when the maximum interstorey drift ratio is 2%. For the frame with an absence of infill walls at the first two storeys (M3), the lateral capacity is 80% lower than that of M2. As the storeys with an absence of infill walls move up, the lateral capacity of the structure becomes increasingly larger and the interstorey drift ratio is decreased. The damage of the pilotis frame with weak ground storey is more serious than that of frames with an absence of infill wall at other storeys. The interstorey drift ratio of M5 is about 16% larger than that of M1. Therefore, this type of irregular vertical infill arrangement should be limited in the design process.

(2) Dynamic time–history analysis was then performed on RC frames with different infill wall materials. The vertical irregularly arranged infill walls lead to the discontinuity of stiffness. The analytical results show that the largest interstorey drift ratio occurs in storeys with an absence of infill walls. For the frames with vertically irregular arrangement, the base storey with an absence of infill walls does the greatest harm to the structures, the interstorey drift ratio of which is the largest (0.95%). The base shear of M2 is the largest among all structures, which is at least three times larger than that of M1. The absence of infill walls at the base storey decreases the base shear by 56–70% compared with M2.

(3) The base shear increases with the increase in the elastic modulus of the infill wall material. For the structures with vertical regularly arranged infill walls, the larger elastic modulus of masonry material can decrease the interstorey drift ratio of the structures. On the contrary, for the models with vertical irregularly arranged infill walls, the larger elastic modulus of masonry material can increase the interstorey drift ratio. Therefore, the disadvantages induced by the elastic modulus of masonry

material, in the frames with vertical irregularly arranged infill, should be considered in the seismic design and assessment.

Author Contributions: Conceptualization, J.K.; methodology, X.W.; software, Y.S. and X.W.; formal analysis, Y.S.; investigation, Z.Z. and Y.Z.; resources, J.K., X.W. and Y.S.; writing—original draft preparation, Y.Z., writing—review and editing, Y.S.; visualization, J.K. and X.W.; supervision, Z.Z.; project administration, J.K.; funding acquisition, J.K. and X.W. All authors have read and agreed to the published version of the manuscript.

Funding: The research is supported by the Scientific Research Fund of the Institute of Engineering Mechanics, China Earthquake Administration (Grand Nos. 2019D09), the National Nature Science Foundation of China (Nos. 51808478 and 51908397), and the Natural Science Foundation of Shandong (Nos. ZR2019QEE033). These supports are greatly appreciated.

Institutional Review Board Statement: Not applicable.

Informed Consent Statement: Not applicable.

Data Availability Statement: The data presented in this study are available on request from the corresponding author.

Acknowledgments: Grateful acknowledgment is given to Shuying Qu and Bo Liu at School of Civil Engineering, Yantai University for the guidance and suggestions on theoretical analyses.

Conflicts of Interest: The authors declare no conflict of interest.

References

1. Ye, L.; Lu, X. Analysis on seismic damage of buildings in the Wenchuan earthquake. *J. Build. Struct.* **2008**, *29*, 1–9.
2. Gong, M.; Lin, S.; Sun, J.; Li, S.; Dai, J.; Xie, L. Seismic intensity map and typical structural damage of 2010 Ms 7.1 Yushu earthquake in China. *Nat. Hazards* **2015**, *77*, 847–866. [CrossRef]
3. Holmes, M. Steel frames with brickwork and concrete infilling. *Proc. Inst. Civ. Eng.* **1961**, *19*, 473–478. [CrossRef]
4. Chaker, A.A.; Cherifati, A. Influence of masonry infill panels on the vibration and stiffness characteristics of R/C frame buildings. *Earthq. Eng. Struct. Dyn.* **1999**, *28*, 1061–1065. [CrossRef]
5. Liauw, T. Tests on multistory infilled frames subject to dynamic lateral loading. *J. Proc.* **1979**, *1979*, 551–564.
6. Angel, R.; Abrams, D.P.; Shapiro, D.; Uzarski, J.; Webster, M. *Behavior of Reinforced Concrete Frames with Masonry Infills*; University of Illinois Engineering Experiment Station: Champaign, IL, USA, 1994.
7. Dafnis, A.; Kolsch, H.; Reimerdes, H.-G. Arching in masonry walls subjected to earthquake motions. *J. Struct. Eng.* **2002**, *128*, 153–159. [CrossRef]
8. Mehrabi, A.B.; Benson Shing, P.; Schuller, M.P.; Noland, J.L. Experimental evaluation of masonry-infilled RC frames. *J. Struct. Eng.* **1996**, *122*, 228–237. [CrossRef]
9. Fiorato, A.E. *An Investigation of the Interaction of Reinforced Concrete Frames with Masonry Filler Walls*; University of Illinois at Urbana-Champaign: Champaign, IL, USA, 1971.
10. BANG Haidong, L. Seismic Performance of RC Frames Considering SSI Effect and Stiffness of Infill Wall. *J. Hunan Univ. Nat. Sci.* **2019**, *46*. [CrossRef]
11. Mondal, G.; Tesfamariam, S. Effects of vertical irregularity and thickness of unreinforced masonry infill on the robustness of RC framed buildings. *Earthq. Eng. Struct. Dyn.* **2014**, *43*, 205–223. [CrossRef]
12. Gong, M.; Zuo, Z.; Wang, X.; Lu, X.; Xie, L. Comparing seismic performances of pilotis and bare RC frame structures by shaking table tests. *Eng. Struct.* **2019**, *199*, 109442. [CrossRef]
13. Kakaletsis, D.J.; Karayannis, C.G. Influence of masonry strength and openings on infilled R/C frames under cycling loading. *J. Earthq. Eng.* **2008**, *12*, 197–221. [CrossRef]
14. Pan, X.; Yan, J.; Wang, Z.; Zou, C. Numerical modeling and seismic evaluation of masonry-infilled reinforced concrete frames retrofitted with carbon fiber–reinforced polymer wraps. *Adv. Struct. Eng.* **2018**, *21*, 1526–1541. [CrossRef]
15. Stavridis, A. *Analytical and Experimental Study of Seismic Performance of Reinforced Concrete Frames Infilled with Masonry Walls*; University of California: San Diego, CA, USA, 2009.
16. Zuo, Z.; Gong, M.; Sun, J.; Zhang, H. Seismic performance of RC frames with different column-to-beam flexural strength ratios under the excitation of pulse-like and non-pulse-like ground motion. *Bull. Earthq. Eng.* **2021**, *19*, 5139–5159. [CrossRef]
17. Stavridis, A.; Shing, P. Finite-element modeling of nonlinear behavior of masonry-infilled RC frames. *J. Struct. Eng.* **2010**, *136*, 285–296. [CrossRef]
18. Zhai, C.; Wang, X.; Kong, J.; Li, S.; Xie, L. Numerical simulation of masonry-infilled RC frames using XFEM. *J. Struct. Eng.* **2017**, *143*, 04017144. [CrossRef]
19. Saneinejad, A.; Hobbs, B. Inelastic design of infilled frames. *J. Struct. Eng.* **1995**, *121*, 634–650. [CrossRef]

20. Thiruvengadam, V. On the natural frequencies of infilled frames. *Earthq. Eng. Struct. Dyn.* **1985**, *13*, 401–419. [CrossRef]
21. Polyakov, S. On the interaction between masonry filler walls and enclosing frame when loaded in the plane of the wall. *Transl. Earthq. Eng.* **1960**, *2*, 36–42.
22. Chrysostomou, C.Z. *Effects of Degrading Infill Walls on the Nonlinear Seismic Response of Two-Dimensional Steel Frames*; Cornell University: New York, NY, USA, 1991.
23. Crisafulli, F.J. Seismic Behaviour of Reinforced Concrete Structures with Masonry Infills. Ph.D. Thesis, University of Canterbury, Christchurch, New Zealand, 1997.
24. Fiore, A.; Netti, A.; Monaco, P. The influence of masonry infill on the seismic behaviour of RC frame buildings. *Eng. Struct.* **2012**, *44*, 133–145. [CrossRef]
25. El-Dakhakhni, W.W.; Elgaaly, M.; Hamid, A.A. Three-strut model for concrete masonry-infilled steel frames. *J. Struct. Eng.* **2003**, *129*, 177–185. [CrossRef]
26. Furtado, A.; Rodrigues, H.; Arêde, A. Calibration of a simplified macro-model for infilled frames with openings. *Adv. Struct. Eng.* **2018**, *21*, 157–170. [CrossRef]
27. *GB50011-2010*; Code for Seismic Design of Buildings. China Architecture and Building Press: Beijing, China, 2010.
28. *GB50010-2010*; Code for Design of Concrete Structures. China Architecture & Building Press: Beijing, China, 2010.
29. Furtado, A.; Rodrigues, H.; Arêde, A.; Varum, H. Simplified macro-model for infill masonry walls considering the out-of-plane behaviour. *Earthq. Eng. Struct. Dyn.* **2016**, *45*, 507–524. [CrossRef]
30. De Risi, M.T.; Di Domenico, M.; Ricci, P.; Verderame, G.M.; Manfredi, G. Experimental investigation on the influence of the aspect ratio on the in-plane/out-of-plane interaction for masonry infills in RC frames. *Eng. Struct.* **2019**, *189*, 523–540. [CrossRef]
31. Ricci, P.; Di Domenico, M.; Verderame, G.M. Experimental assessment of the in-plane/out-of-plane interaction in unreinforced masonry infill walls. *Eng. Struct.* **2018**, *173*, 960–978. [CrossRef]